ELSEVIER

Trends and perspectives in solid-state wetting / Mouillage solide–solide : tendances et perspectives

Time-dependent analysis of agglomerating Pt thin films on YSZ single crystals

CrossMark

Analyse temporelle de l'agglomération de films minces de Pt sur YSZ monocristallin

Henning Galinski [a,b,*], Thomas Ryll [a], Lukas Schlagenhauf [a], Iwan Schenker [a], Ralph Spolenak [b], Ludwig J. Gauckler [a,c]

[a] *Nonmetallic Inorganics Materials, Department of Materials, ETH Zurich, Wolfgang-Pauli-Str. 10, CH-8093 Zurich, Switzerland*
[b] *Laboratory of Nanometallurgy, Department of Materials, ETH Zurich, Wolfgang-Pauli-Str. 10, CH-8093 Zurich, Switzerland*
[c] *International Institute for Carbon Neutral Energy Research (WPI-I2CNER), Kyushu University, 744 Moto-oka, Nishi-ku, Fukuoka 819-0395, Japan*

ARTICLE INFO

ABSTRACT

The controlled assembly of nanostructures via shape instability mechanisms is a potential alternative to traditional top-down processes like e-beam lithography for nanostructuring surfaces. In this contribution, the dynamics of the nanostructures' assembly via thin film agglomeration have been analyzed. Pt thin films with a thickness of 50 nm were deposited via magnetron sputtering on yttria-stabilized zirconia (YSZ) single crystals and subjected to heat treatments at 1023 K for times ranging from 10 to 130 min. The morphological evolution of Pt thin films has been investigated by means of scanning electron microscopy (SEM) and atomic force microscopy (AFM), obtaining the hole growth dynamics and morphological parameters like the lateral correlation length and the nanostructures' Minkowski functionals. The experimentally obtained morphology evolution is compared to the simulated evolution of thin film structures resulting from a cell dynamical system (CDS) model. Three main observations have been made. (i) The hole radius is found to scale as function of time t with a rate proportional to $t^{-\frac{3}{4}}[\log^3 t]$. This is in agreement with Srolovitz's instability theory describing hole growth predominated by surface diffusion. (ii) The morphological evolution of the Pt thin films has been analyzed as function of time t by means of Minkowski measures and the lateral correlation length. A discontinuity in the lateral correlation length and a significant deviation of the Minkowski functionals from the expected Gaussian behavior was found to be coupled with the coalescence of holes. (iii) By using the Ginzburg–Landau equation for the description of the fundamental diffusion process, the CDS model allows a computational reproduction of the experimentally obtained film morphologies in the early stages of agglomeration.

© 2013 Académie des sciences. Published by Elsevier Masson SAS. All rights reserved.

RÉSUMÉ

La nano-structuration de films minces par des mécanismes d'instabilités spatiales est une alternative potentielle aux processus traditionnels dits « top-down », comme par exemple la lithographie à faisceau d'électrons. Dans cette contribution, nous analysons la dynamique

* Corresponding author at: Laboratory of Nanometallurgy, Department of Materials, ETH Zurich, Wolfgang-Pauli-Str. 10, CH-8093 Zurich, Switzerland.
E-mail address: henning.galinski@mat.ethz.ch (H. Galinski).

de la structuration de films minces par agglomération. Pour cela, des films minces de Pt d'une épaisseur de 50 nm ont été déposées sur des substrats monocristallins de zircone yttriée (YSZ) par pulvérisation magnétronique. La déposition a été suivie d'un traitement thermique à 1023 K pendant 10 à 130 minutes. L'évolution morphologique des films minces de Pt a été étudiée par microscopie électronique à balayage et par microscopie à force atomique. Cela a permis de déterminer la dynamique de croissance des cavités dans le film ainsi que des paramètres morphologiques comme la distance de corrélation latérale et les fonctionnelles de Minkowski. L'évolution morphologique obtenue expérimentalement a été comparée aux structures de films minces déterminées par des simulations de dynamique cellulaire. Trois observations ont été faites. (i) Le rayon des cavités dépend du temps t, avec un taux de croissance proportionnel à $t^{-\frac{3}{4}}[\log^3 t]$, ce qui est en accord avec la théorie d'instabilité de Srolovitz, décrivant la croissance de cavités dominée par une diffusion superficielle. (ii) L'évolution morphologique des films minces de Pt a été analysée en fonction du temps à l'aide des mesures de Minkowski et de la distance de corrélation latérale. Une discontinuité de la distance de corrélation latérale couplée à la coalescence des cavités a été trouvée, ainsi qu'une déviation significative des fonctionnelles de Minkowski du comportement gaussien attendu. (iii) En utilisant l'équation de Ginzburg–Landau comme équation de diffusion fondamentale, les simulations de dynamique cellulaire ont permis de reproduire les morphologies des films minces pendant la phase initiale de l'agglomération.

1. Introduction

The functionality of many new technological devices derives from the usage of nano-structured or nano-patterned materials. In most cases, these nanostructures are produced by top-down lithography processes. Although widely used, lithography processes are expensive and the structurable area is often limited, like for example in the case of e-beam lithography. Therefore, alternative pathways to manipulate and assemble nanomaterials by bottom-up processes have been subjected to intensive research in the past few years [1–4].

One promising approach is the controlled assembly of nanostructures via shape instability mechanisms like thin film agglomeration (solid-state dewetting) [5,6], ion beam radiation [7,8] or dealloying and phase separation [9,10]. In case of thin film agglomeration or solid-state dewetting, the pattern formation is driven by the minimization of the systems' free energy F due to an external perturbation like annealing, Joule heating, or ion bombardment. The reconfiguration is accomplished by mass transport that is enhanced at surface regions of maximal curvature or a large surface stiffness. The regions of maximal curvature coincide with the triple junctions of the thin film (i.e. lines where three grain boundaries meet) [11]. This concept was first introduced by Mullins [11] for thermal grooving and thermal pinning at grain boundaries and was later extended by Brandon and Bradshaw [12] and Srolovitz et al. [13,14] to describe the decomposition of a homogeneous crystalline surface via hole growth. Thin film agglomeration has been subjected to research under several aspects: thermodynamics and kinetics [5,15,16], mass transport via surface diffusion [5,12,17], mass transport via evaporation and sublimation [18], impact of surface energy anisotropies and adhesion [19–23], fingering instabilities [24,20,25,26], Ostwald ripening of islands [27], hole pattern [28] and hillock formation [29–35].

Most of the fundamental theoretical work has been carried out by Srolovitz and Safran, who developed a complete stability theory for thin films covering kinetics [14] and energetics [13]. A detailed review of current progressions in the field can be found in Ref. [36].

Recently, significant attention has been drawn to using thin film agglomeration on pre-patterned surfaces [1,3,2,4,37] in order to achieve self-assembled structures with a defined periodicity. By utilizing the anisotropic movement of dewetting fronts beyond that, it is deemed a promising way to obtain repetitive nanostructures with well-defined orientations [1,38]. The main objective of this paper is to obtain a general understanding of the physics behind the macroscopical changes in the morphology of the thin film as a function of time. The investigation focuses on the determination of the operative transport mechanism and its time scaling. Furthermore, the morphological evolution of the thin film is analyzed by morphological measures such as the surface coverage, the roughness, and the lateral correlation length. Additionally, more sophisticated surface descriptors such as the Minkowski functionals have been chosen to analyze the time-dependent spatial evolution of the thin film's morphology. In order to gain a deeper understanding of the involved physical mechanisms during thin film agglomeration, a cell dynamic simulator has been designed, aiming at a qualitative reproduction of the pattern formation determined experimentally.

This paper is structured as follows: Section 2 introduces the three most important time-dependent models for thin film agglomerations. Section 3 deals with the experimental framework. In Section 4, detailed experimental and computational results are presented and discussed. The final Section 5 summarizes the findings and conclusions.

2. Theoretical background

2.1. Agglomeration kinetics

During deposition of metal thin films via sputtering or other physical vapor deposition techniques, the kinetic energy E_{kin} of the deposited atoms generally exceeds their thermal energy E_{ther}. For the deposited film, this results in a metastable configuration that tends to equilibrate, once subjected to temperature by annealing, Joule heating or radiation. The equilibration process leads to shape instabilities driven by the minimization of the system's free energy F. The change of F defines the systems' chemical potential μ. The total free energy F of an incompressible solid with N atoms and surface tension $\boldsymbol{\sigma}$ reads

$$F = (\mu_0 - P\Omega) \cdot N + \iint \boldsymbol{\sigma}\left(\frac{\partial z}{\partial x}, \frac{\partial z}{\partial y}\right) \tag{1}$$

whereby μ_0 is the chemical potential, P the pressure and Ω the molar volume per atom. In the majority of cases, the determination of F is intricate. Therefore, it often suffices to describe the increase in chemical potential μ per atom solely as a function of the surface's curvature K,

$$\mu(K) = K\gamma_s\Omega \tag{2}$$

where γ_s is the surface-free energy per unit area. The net flux $\mathbf{j}$ of diffusing atoms is defined as the gradient of chemical potential and, hence, is associated with the gradient of curvature via

$$\mathbf{j} = -\frac{D_s}{k_B T} \cdot \mathbf{grad}\,\mu = -\frac{D_s \gamma_s \Omega}{k_B T} \cdot \mathbf{grad}\,K \tag{3}$$

where D_s is the surface mass-transport coefficient. Based on these assumptions, several models have been developed in the field of thin film agglomeration, which establish a relation between the growing hole radius r and the annealing time t. The first model has been derived by Brandon and Bradshaw [12]. It states that the time-evolution of the mean hole radius $\langle r \rangle$ is equal to the product of D_s and the kinetic parameters of the film [12]:

$$\frac{dr}{dt} = \frac{\left(\frac{2}{5}\right)^{3/5} B \cdot \pi^{1/5}}{h^{3/2}\left(\frac{B \cdot t}{h^{3/2}}\right)^{3/5}} \tag{4}$$

$B = \frac{D_s \Omega^2 \gamma_s \nu}{k_B T}$, thereby ν is the surface density of sites, h the film thickness. A detailed derivation and discussion of the boundary conditions of the Brandon–Bradshaw model can be found in Refs. [12] and [5].

In contrast to the Brandon–Bradshaw model, Jiran and Thompson have proposed a model [39] that adapts to the morphological evolution and void growth found experimentally for fingering instabilities [39]. Jiran and Thompson predict that the growth rate of the hole radius r is constant in time t and depends inversely cubic on the film thickness h,

$$\frac{dr}{dt} = \frac{2D_0 \Omega^2 \gamma_s \exp[-E_a/k_B T]}{k_B T \pi h^3} \tag{5}$$

In the work of Jiran and Thompson, the perturbation are not associated with static polycrystalline defects like triple junctions, but to the free surface of the line edge of the deposited metal strip.

The model of Brandon and Bradshaw has been extended by Srolovitz [14], whereby the hole evolution is considered to be impacted either by surface-diffusion kinetics or by evaporation–condensation kinetics. The growth rate for surface-diffusion kinetics is given by:

$$\frac{dr}{dt} = V B^{\frac{1}{4}} t^{-\frac{3}{4}} \left\{\ln^3\left[Bt(\tan\theta/h)^4\right] + \cdots\right\} \tag{6}$$

where V is a free fitting parameter. The model considers the influence of the substrate by taking into account the wetting angle θ. It is reported that the critical ratio $\tan\theta/h$ of the film thickness h and the wetting angle θ triggers hole growth [14]. For small t values, the functional form of Eq. (6) is similar to the parabolic time scaling of $r \propto t^{\frac{1}{2}}$ found by Bussmann [19] using KMC simulations. It is noteworthy that this geometrical parameter might be replaced by the truncation depth of the film using the generalized Wulff–Kaishew equation [40].

3. Experimental

3.1. Sample preparation and characterization

The Pt/YSZ (single-crystalline) system is immiscible and a chemical inert interface is formed for all temperatures below 1273 K [41]. Pt layers of 50 nm in thickness were deposited at room temperature by magnetron sputtering

($p_{\text{base}} = 10^{-7}$ mbar) onto the single-crystalline substrates that were pre-cleaned using isopropanol. The substrates coated with the thin platinum film were annealed in a Nabertherm L3/11/P320 muffle furnace at 1023 K for different times ranging from 10 to 130 min. The heating and cooling rate for all samples was chosen to 3 K/min. For a balanced heat distribution on the sample surface, the samples were covered by an alumina cap and a cage of alumina. The additional contribution to the annealing time t during heating and cooling is determined by:

$$t = \int_0^{t_c} \exp\left[\frac{E_a}{R} \left(\frac{1}{T_a} - \frac{1}{T(\acute{t})} \right) \right] d\acute{t} \tag{7}$$

whereby t_c is the duration of the heating, E_a is the activation energy of the agglomeration process, R is the gas constant, T_a is the desired temperature, and $T(\acute{t})$ is the temperature as a function of time during heating or cooling [42]. The annealing temperature is well below the melting temperature of platinum $T_M = 2042$ K, hence volume diffusion of Pt in Pt is prohibited.

The morphology of the samples was studied via high resolution AFM, using a Mobile S (Nanosurf) and a Topometrix 2000. The Minkowski functionals have been calculated from the acquired images using a square-marching algorithm developed by Mantz et al. [43]. The Minkowski functionals m_n in $2D$ are surface descriptors, which capture the covered area m_1, the boundary length m_2, and the difference between the number of holes and the number of connected components, the Euler number m_3. Minkowski functionals are capable of detecting higher orders of spatial correlation and are suited to test spatial structures for non-Gaussian behavior or features [44,45,43], as they provide a unique analytical solution for Gaussian random fields. The Minkowski functionals are given by:

$$m_0(h) = \frac{1}{2}\left(1 - \text{erf}\left(\frac{h}{\sqrt{2}\sigma} \right) \right) \tag{8a}$$

$$m_1(h) = \frac{k}{\sqrt{8\pi}} \exp\left(-\frac{h^2}{2\sigma^2} \right) \tag{8b}$$

$$m_2(h) = \frac{hk^2}{\sqrt{2\pi^3\sigma^2}} \exp\left(\frac{h^2}{2\sigma^2} \right) \tag{8c}$$

whereby σ^2 is the film's roughness and k corresponds to the second derivative of the covariance in 0. For the sake of simplicity, effective measures for $s(h), u(h), \kappa(h)$ can be defined [46,43,45] using:

$$s(h) = -\frac{\partial m_0}{\partial h} \cdot \frac{1}{2\pi \cdot m_1(h)} \tag{9a}$$

$$u(h) = -\log\left(-2\pi \cdot m_1(h)\right) \tag{9b}$$

$$\kappa(h) = \frac{m_2(h)}{2m_1(h)} \tag{9c}$$

and

$$s(h) = s_0 \tag{10a}$$

$$u(h) = u_0 + u_2 h^2 \tag{10b}$$

$$\kappa(h) = \kappa_1 h \tag{10c}$$

This definition is beneficial, as only two sensitive parameters are required to test experimental structures for non-Gaussian behavior. These two parameters are given by:

$$X := \frac{s_0 \exp\left(-2u_0\right)}{\kappa_1} = \frac{\pi}{2} \quad \text{and} \quad Y := \frac{\kappa_1 s_0}{u_2} = \frac{2}{\pi^2} \tag{11}$$

A detailed description of this procedure is given by Mecke et al. [43,45]. The coverage and hole size distributions were measured with a FESEM Leo1530 (Zeiss) equipped with a four-quadrant back-scatter (QBSD) detector. This detector eliminates topographic information and produces a pure composition signal that is most suitable to produce binary images that can easily be fed into common image analysis algorithms. In order to increase the statistical significance of the obtained data sets, matrices of 5×5 images have been acquired and combined using the Microsoft Image Composite Editor 1.2.
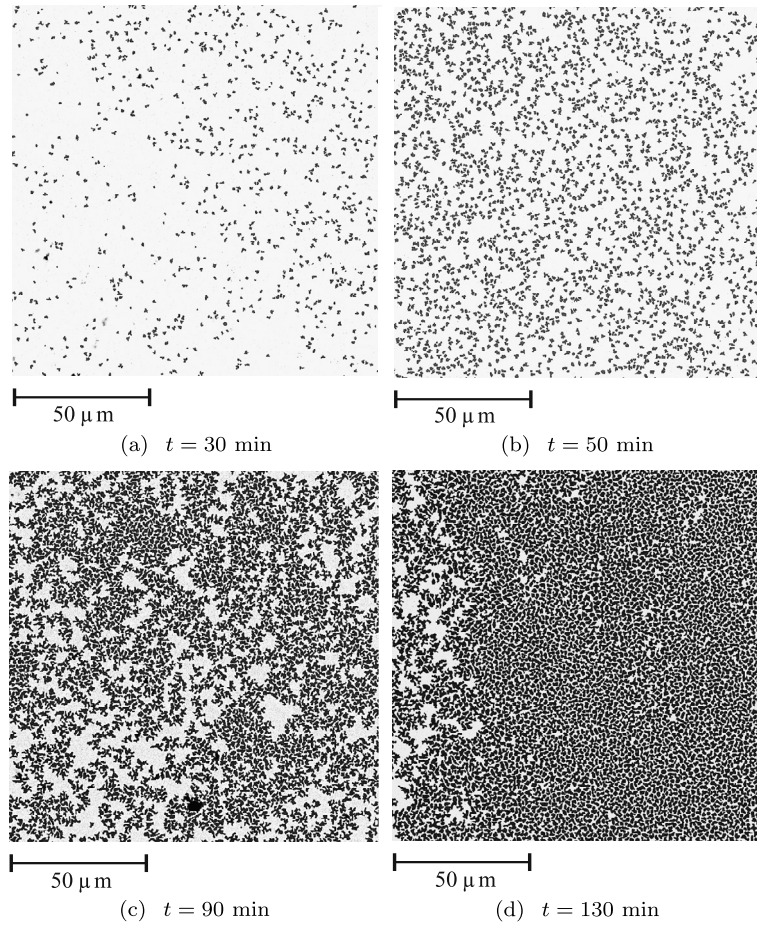
Fig. 1. SEM images of different agglomeration stages with corresponding annealing times t of Pt on YSZ (thickness 50 nm, annealed in air at 1023 K). (a) $t = 30$ min, onset of rupture and hole formation; (b) $t = 50$ min, further nucleation of holes and hole growth; (d) and (c) $t \geqslant 90$ min, hole growth and coalescence of holes.

3.2. Cell dynamic system model

In analogy to pattern formation and phase separation in block copolymers [47–51], a conventional cell dynamic system (CDS) model approach has been chosen to reproduce the experimentally observed agglomeration pattern. This approach is based on previous findings, which clearly indicated that the mechanism of rupture of thin platinum films is based on defect-induced nucleation of holes. The rupture mechanism is dominated by nucleation at randomly distributed perturbation sites. It has been shown by Oono and Puri [52], that such a nucleation regime starting with a metastable system can be modeled by a cell dynamic system model using a discretized form of the Ginzburg–Landau equation for the segregation of the system. This approach has been adapted to the present case. The thickness h is identified with the order parameter ψ of the system ($h = \psi$). The order parameter ψ_{nc} at time $t + 1$ is given by

$$\psi_{nc}(t+1, n) = f\big(\psi(t, n)\big) + D \cdot \big[\langle\!\langle \psi(t, n)\rangle\!\rangle - \psi(t, n)\big] \tag{12}$$

where $f = \alpha \cdot \psi / (1 + \psi \sqrt{\alpha^2 - 1})$ is a generic map function, which reproduces the two minima in an asymmetric double-well potential. This definition of the cell dynamic system uses the discretized time-dependent Ginzburg–Landau equation to map the agglomeration pattern at time t to the pattern at time $t + 1$. It is noteworthy that a CDS model does not require a specific formulation of the system's free energy [53]. D is the diffusion constant and $\langle\!\langle X \rangle\!\rangle$ denotes the averaging over the nearest (nn) and the next-nearest neighbors (nnn) given by:

$$\langle\!\langle X \rangle\!\rangle = \frac{1}{8} \sum_{i \in nn} X_i + \frac{1}{16} \sum_{i \in nnn} X_i \tag{13}$$

The discrete Laplacian $\langle\!\langle X \rangle\!\rangle - X$ is calculated on the Moore neighborhood of each cell. The simulations are performed on a GPU device using CUDAfy V1.12. The grid had a size of 1024×1024 positions and periodic boundary conditions. For
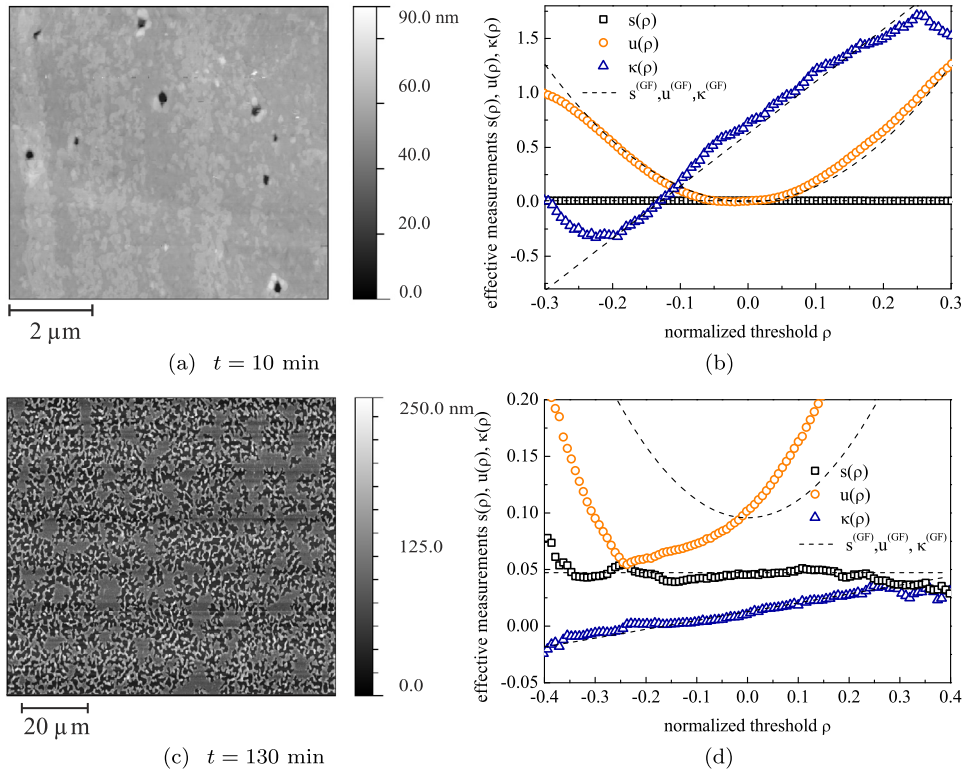
Fig. 2. (a) AFM image of the thin film morphology of Pt on YSZ after 10 min annealing at 1023 K. (b) Effective measures $s(\rho), u(\rho), \kappa(\rho)$ with $\rho = 1 - \frac{2h}{h_{max}}$ determined from Minkowski functionals according to Eq. (10), which are in good agreement with a Gaussian model (dashed lines). (c) AFM image of the thin film morphology of Pt on YSZ after 130 min annealing at 1023 K. (d) Effective measures $s(\rho), u(\rho), \kappa(\rho)$ determined from the Minkowski functionals according to Eq. (10), with a significant deviation from the Gaussian model (dashed lines).

the initial configuration, the order parameter ψ is set to 0 and 24 perturbation sites are created at random locations on the grid. Each perturbation site contains 25 cells, consisting of a central cell surrounded by its first and second Moore neighborhood. The inner cell's order parameter is normally distributed around a mean $\psi_0 = 0.05$, the order parameter of the first Moore neighborhood is normally distributed around a mean $\psi_0 = -0.005$, and the order parameter of the second Moore neighborhood is normally distributed around a mean $\psi_0 = -0.005$. The standard deviation is set to $\sigma = 0.01$ everywhere. The overall mean order parameter of the perturbation site is $\psi_0 = -0.07$. Besides the local perturbations, the order parameter is chosen to be isotropic and contributions due to the polycrystallinity of the sample, such as grain boundaries, have been ignored.

4. Results and discussion

4.1. Pattern formation and kinetics

For all agglomerated Pt thin films, annealed isothermally at $T = 1023$ K for different annealing times ranging from 10 to 130 min, the expected stages of film agglomeration were reproduced. In Figs. 1(a)–1(c), the experimental stages for one set of isothermally treated samples with an initial film thickness of $h = 50$ nm are shown. Figs. 1(a) and 1(b) depict the nucleation regime where holes form and break the symmetry of the original film. The hole density doubles between $t = 10$ min and $t = 30$ min from $\rho = 0.03/\mu m^2$ to $\rho = 0.06/\mu m^2$. With increasing annealing time, the holes continue to grow, begin to interact and finally impinge, which results in the formation of a continuous network, see Fig. 1(d). The resulting surface morphologies are similar to patterns resulting from a decomposition of binary mixtures [54]. The coalescence of holes is accompanied by an increasing contour length (Fig. 1(c)).

In accordance with previous findings on the agglomeration of isochronically annealed Pt thin films on dielectric substrates [5], we assume that the rupture mechanism is dominated by nucleation in the spinodal regime [55]. Using the concepts derived in Section 3.1, the experimentally revealed surface morphologies are analyzed via Minkowski functionals. The morphologies determined by AFM for two different annealing times are shown in Figs. 2(a) and 2(c). For each annealing time, the corresponding Minkowski functionals have been calculated and tested for the non-Gaussian behavior by fitting the calculated effective measures for $s(h), u(h), \kappa(h)$ (Eq. (9)) with their predicted forms for a Gaussian random field, see Eq. (10). The observed shapes of $s(h), u(h), \kappa(h)$, plotted in Figs. 2(b) and 2(d), show a pro-
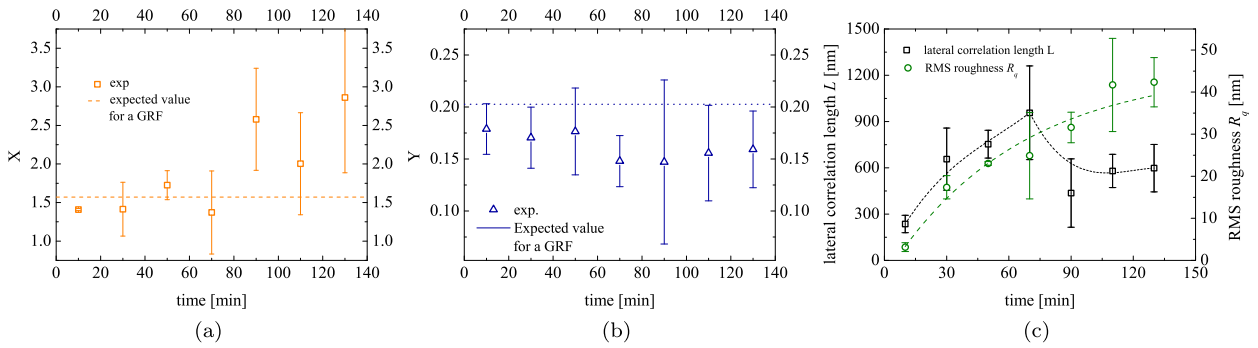
Fig. 3. (a)–(b) The figure depicts, for each annealing time t, the consistency check for X and Y as given by Eq. (11) for a Gaussian random field. A significant deviation from the expected X value is found for $t > 90$ min, all other values are in good agreement with the expected values for X and Y. (c) Determined lateral correlation length L and R_q roughness as a function of annealing time t at 1012 K. The dashed lines serve as a guide for the eye.

nounced resemblance with the expected analytical expressions for a Gaussian random field. Although in the case of long annealing times $t = 130$ min (Fig. 2(d)) a significant deviation from the expected parabola shape for $u(h)$ is found. In order to test the experimental data on inconsistencies with the Gaussian model, X and Y (Eq. (11)) have been determined from the obtained fitting parameters. The evolution of X and Y as function of t is shown in Figs. 3(a) and 3(b), respectively. The theoretically expected values for X and Y are depicted as dashed lines. It is found that for annealing times $t > 90$ min, the parameter X deviates significantly from the expected Gaussian behavior, which is coupled to the coalescence of holes. This coincides with a discontinuity of the lateral correlation length, while the roughness of the thin film is continuously increasing, see Fig. 3(c). Hence, it can be substantiated with the help of the obtained Minkowski functionals and the correlation length, that once a critical hole size is reached the growth of a single hole cannot be treated independently anymore and the interaction with neighboring holes has to be taken into account. The nature of this interaction is probably based on a long-range interaction like the cohesion of the film or a strain field.

These finding should have a direct impact on the hole's growth rate, as one would intuitively expect a decreasing kinetics with the onset of a multiple hole interaction. Hence, in order to determine the growth rate of holes, the mean hole radius $\langle r \rangle$ has been determined from the captured QBSD images for various annealing times by state-of-the-art image analysis [5]. As shown in Ref. [5], the hole radius r is normally distributed. By using matrices of 5×5 auto-correlated SEM images, the field of view and the number of measured holes has been increased and hence the standard deviation of the mean hole radius $\langle r \rangle$ has been significantly reduced. The mean hole radius $\langle r \rangle$ is plotted as a function of t in Fig. 4 and compared to the hole growth models introduced in Section 2.1, Eqs. (4)–(6) (dashed lines). Eqs. (4) and (5) do not contain any fitting parameter, whereas Eq. (6) was fitted to the experimental data using the fitting parameter V. The diffusion constant D_s was calculated using the activation energy E_a and the prefactor D_0 from Ref. [5]. The wetting angle $\theta = 65.8°$ has been determined via image analysis of focused ion beam cross-sections of the agglomerated thin film. Fig. 4 shows that the Srolovitz model (Eq. (6)) nicely reproduces the experimental data using $V = 0.045$, suggesting that the mean hole radius presents a time scaling of $t^{-\frac{3}{4}}[\log^3 t]$. Furthermore, the Brandon–Bradshaw model applies for annealing times $t \geqslant 4200$ s, but the scaling behavior of the Jiran–Thompson model cannot be reproduced. The observed discrepancy between the model of Jiran and Thompson and our experimental data can be explained by the differences in the experimental conditions. In
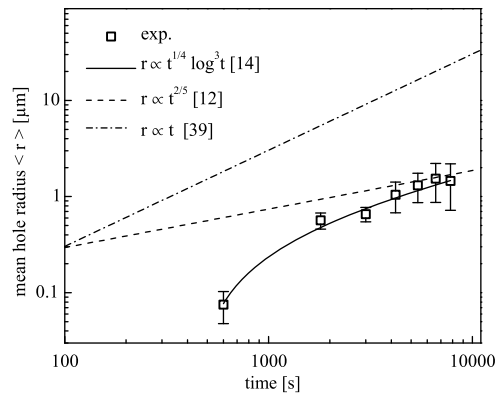

Fig. 4. Log–log plot of the mean hole radius $\langle r \rangle$ as function of the annealing time t for Pt thin films (50 nm) on YSZ annealed at 1023 K. The obtained temporal evolution of r is in good agreement with the Srolovitz model $\dot{r} \propto t^{-\frac{3}{4}}[\log^3 t]$, the predicted rates for the Brandon–Bradshaw model $\dot{r} \propto t^{-\frac{3}{5}}$ and Jiran–Thompson model $\dot{r} = $ const are plotted as well (dashed lines).
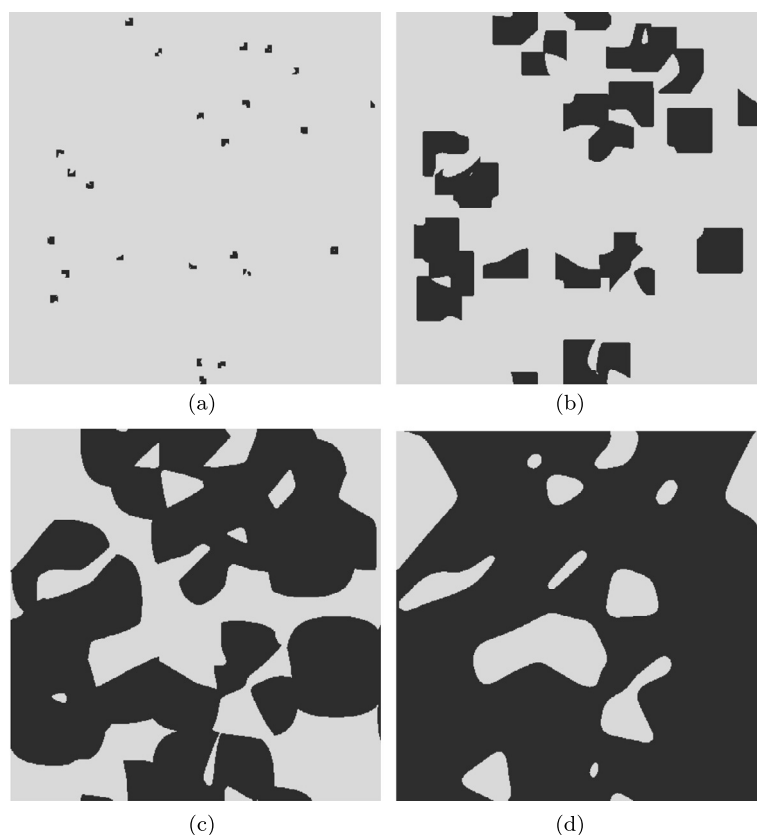
Fig. 5. Simulated agglomeration pattern obtained using the CDS model (1024 × 1024 px). (a)–(d) show the hole (black) pattern formation as a function of the simulation time. The obtained morphologies evolve as a function of the simulation time, in quantitative agreement with the experiments.

the work of Jiran and Thompson, the perturbations are not associated with static polycrystalline defects like triple junctions, but with the free surface of the line edge of the deposited metal strip.

In analogy to Srolovitz et al. [14], we conclude from the found time scaling of the hole growth shown in Fig. 4 and the observed deviation from a Gaussian behavior that the hole growth at short times is enhanced and dominated by the film's aspect ratio. For long annealing times, the kinetics is decelerated due to an increasing impact of long-range interactions, like surface undulations or strain fields, on the kinetics.

4.2. CDS simulation

In order to gain a general understanding of the mechanisms of pattern formation via agglomeration, a cell dynamical system has been defined, which satisfies the main experimentally observed initial conditions. The rupture of a metastable nanocrystalline thin film is realized by randomly placed nucleation seeds, with a normally distributed order parameter ψ. This corresponds to a rupture due to heterogeneously nucleating nonlinear perturbations, which are associated with the nucleation of barrierless defects in the film. The diffusion-controlled hole formation that depends on the curvature or surface stiffness of the thin film is captured by the time-dependent Ginzburg–Landau equation and its diffusion coefficient $D = 0.45$. In accordance with previous findings [5], we interpret the film's agglomeration as nucleation in the spinodal regime [56], whereby the pattern formation is controlled by a double-well potential f with $\alpha = 1.25$. In Fig. 5, the different stages of the thin film agglomeration, simulated by the CDS model, are shown. The chosen approach reproduces the experimentally observed transition from a dense film to single isolated particles, see Figs. 5(a) and 5(b). In order to quantitatively validate the morphological resemblance between the experimental and computational patterns, the dewetted area α and the contour length l have been chosen as morphological parameters. By doing so, the time-scaling properties of the hole growth and hole coalescence have been calculated for the simulated and the experimental data. The dewetted area α and the contour length l capture two main pattern characteristics: the continuous–discontinuous transition of the metastable film and the hole growth kinetics. The measured dewetted area α for the experimental and the simulated surfaces are shown in Fig. 6(a). The simulated tanh profile of α coincides with the observed continuous–discontinuous transition of the metastable film and the found hole growth kinetics. The contour length l for the experimental and the simulated pattern follow both the same trend and the transition from a percolating network to single particles is reproduced quantitatively. In Fig. 6(b), the simulated contour length has been rescaled, such that 1 px = 9.84 nm. The observed pattern evolution of the experimental and
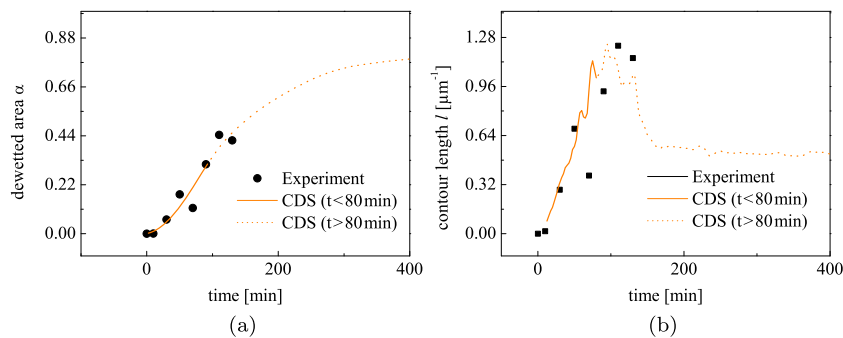
Fig. 6. (a) Plot of the dewetted area α vs. time t for the experimentally obtained and the simulated Pt thin film morphologies. Part (b) depicts the measured contour length l as function of time t for both the experimental and simulated morphologies. After the point at which the morphologies deviate from a Gaussian random field, the validity of the simulation has to be verified (dotted line).

simulated data are in good accordance. However, the validity of the simulations for long annealing times has to be verified as a long-range correlation of the order parameter has not been considered. Besides this long-range correlation, in a next step the polycrystallinity of nature of the metal thin film has to be taken into account. This can be realized by considering contributions of the grain boundary energies to the free energy of the system or by accounting for the anisotropic kink formation energies [29] using an anisotropic diffusion coefficient.

5. Conclusion

In essence, it has been shown that the kinetics of thin film agglomeration is enhanced for short annealing times and decelerates with increasing t, due to a long-range interaction that is coupled to the onset of the coalescence and of the interaction of holes. This finding is in good accordance with the theoretical predictions made by Srolovitz et al. [14]. Furthermore, it has been found that the hole radius r scales as a function of time t with a rate proportional to $t^{-\frac{3}{4}}[\log^3 t]$. This is in agreement with the proportionality given by Srolovitz's instability theory for holes growing predominantly by surface diffusion. The morphological evolution of the Pt thin films has been analyzed as function of time t by means of Minkowski measures and the lateral correlation length. Coupled to the coalescence of holes, a discontinuity of the lateral correlation length and a significant deviation of the Minkowski functionals from the expected Gaussian behavior was found. By using a Ginzburg–Landau approach as a fundamental diffusion equation, the CDS model allows a computational reproduction of the experimentally obtained film morphologies in the early stages of agglomeration. This suggests that the CDS model constitutes an applicable and efficient approach to study and predict the pattern formation process in agglomerating thin metal films.

Acknowledgements

References

[1] J. Ye, C.V. Thompson, Templated solid-state dewetting to controllably produce complex patterns, Adv. Mater. 23 (13) (2011) 1567–1571, http://dx.doi.org/10.1002/adma.201004095.

[2] W.K. Choi, T.H. Liew, H.G. Chew, F. Zheng, C. Thompson, Y. Wang, M.H. Hong, X.D. Wang, L. Li, J. Yun, A combined top-down and bottom-up approach for precise placement of metal nanoparticles on silicon, Small 4 (3) (2008) 330–333, http://dx.doi.org/10.1002/smll.200700728.

[3] A.L. Giermann, C.V. Thompson, Solid-state dewetting for ordered arrays of crystallographically oriented metal particles, Appl. Phys. Lett. 86 (12) (2005) 121903, http://dx.doi.org/10.1063/1.1885180.

[4] C.M. Müller, F.C.F. Mornaghini, R. Spolenak, Ordered arrays of faceted gold nanoparticles obtained by dewetting and nanosphere lithography, Nanotechnology 19 (48) (2008) 485306.

[5] H. Galinski, T. Ryll, P. Elser, J.L.M. Rupp, A. Bieberle-Hütter, L.J. Gauckler, Agglomeration of Pt thin films on dielectric substrates, Phys. Rev. B 82 (2010) 235415, http://dx.doi.org/10.1103/PhysRevB.82.235415.

[6] T. Ryll, H. Galinski, L. Schlagenhauf, P. Elser, J.L.M. Rupp, A. Bieberle-Hutter, L.J. Gauckler, Microscopic and nanoscopic three-phase-boundaries of platinum thin-film electrodes on YSZ electrolyte, Adv. Funct. Mater. 21 (3) (2011) 565–572, http://dx.doi.org/10.1002/adfm.201001729.

[7] A.S. El-Said, R.A. Wilhelm, R. Heller, S. Facsko, C. Lemell, G. Wachter, J. Burgdörfer, R. Ritter, F. Aumayr, Phase diagram for nanostructuring caf$_2$ surfaces by slow highly charged ions, Phys. Rev. Lett. 109 (2012) 117602, http://dx.doi.org/10.1103/PhysRevLett.109.117602.

[8] M. Holmes-Cerfon, W. Zhou, A.L. Bertozzi, M.P. Brenner, M.J. Aziz, Development of knife-edge ridges on ion-bombarded surfaces, Appl. Phys. Lett. 101 (14) (2012) 143109, http://dx.doi.org/10.1063/1.4755838.

[9] D. Mukherji, G. Pigozzi, F. Schmitz, O. Näth, J. Rösler, G. Kostorz, Nano-structured materials produced from simple metallic alloys by phase separation, Nanotechnology 16 (10) (2005) 2176.

[10] T. Ryll, H. Galinski, L. Schlagenhauf, F. Rechberger, S. Ying, L.J. Gauckler, F.C.F. Mornaghini, Y. Ries, R. Spolenak, M. Döbeli, Dealloying of platinum–aluminum thin films: Electrode performance, Phys. Rev. B 84 (2011) 184111, http://dx.doi.org/10.1103/PhysRevB.84.184111.

[11] W.W. Mullins, Theory of thermal grooving, J. Appl. Phys. 28 (3) (1957) 333–339, http://dx.doi.org/10.1063/1.1722742.

[12] R. Brandon, F. Bradshaw, The mobility of the surface atoms of copper and silver evaporated deposits, Technical Report, Royal Aircraft Establishment, Farnborough, England, 1966, p. 38.

[13] D.J. Srolovitz, S.A. Safran, Capillary instabilities in thin films. I. Energetics, J. Appl. Phys. 60 (1) (1986) 247–254, http://dx.doi.org/10.1063/1.337689.

[14] D.J. Srolovitz, S.A. Safran, Capillary instabilities in thin films. II. Kinetics, J. Appl. Phys. 60 (1) (1986) 255–260, http://dx.doi.org/10.1063/1.337691.

[15] D.J. Srolovitz, M.G. Goldiner, The thermodynamics and kinetics of film agglomeration, JOM 47 (1995) 31–36.

[16] F. Genin, W. Mullins, P. Wynblatt, Capillary instabilities in thin films: A model of thermal pitting at grain boundary vertices, Acta Metall. Mater. 40 (12) (1992) 3239–3248, http://dx.doi.org/10.1016/0956-7151(92)90037-F.

[17] E.G. Gontier-Moya, I. Beszeda, F. Moya, Comparisons of parameters involved in mass transport and desorption at the surface of noble metals and sapphire, in: Proceedings of the 22nd European Conference on Surface Science, Surf. Sci. 566–568 (Part 1) (2004) 148–154, http://dx.doi.org/10.1016/j.susc.2004.05.037.

[18] A. Chame, O. Pierre-Louis, Dewetting of solid films with substrate-mediated evaporation, Phys. Rev. E 85 (2012) 011602, http://dx.doi.org/10.1103/PhysRevE.85.011602.

[19] E. Bussmann, F. Cheynis, F. Leroy, P. Müller, O. Pierre-Louis, Dynamics of solid thin-film dewetting in the silicon-on-insulator system, New J. Phys. 13 (4) (2011) 043017.

[20] M. Dufay, O. Pierre-Louis, Anisotropy and coarsening in the instability of solid dewetting fronts, Phys. Rev. Lett. 106 (10) (2011) 105506, http://dx.doi.org/10.1103/PhysRevLett.106.105506.

[21] J. Goniakowski, C. Mottet, C. Noguera, Non-reactive metal/oxide interfaces: from model calculations towards realistic simulations, Phys. Status Solidi B 243 (11) (2006) 2516–2532, http://dx.doi.org/10.1002/pssb.200541456.

[22] C. Stöcker, A. Voigt, The effect of kinetics in the surface evolution of thin crystalline films, in: Proceedings of the Fifth Workshop on Modeling in Crystal Growth – IWMCG-5, J. Cryst. Growth 303 (1) (2007) 90–94, http://dx.doi.org/10.1016/j.jcrysgro.2006.11.246.

[23] E. Dornel, J.-C. Barbé, F. de Crécy, G. Lacolle, J. Eymery, Surface diffusion dewetting of thin solid films: Numerical method and application to Si/SiO2, Phys. Rev. B 73 (11) (2006) 115427, http://dx.doi.org/10.1103/PhysRevB.73.115427.

[24] J. Ye, C.V. Thompson, Anisotropic edge retraction and hole growth during solid-state dewetting of single crystal nickel thin films, Acta Mater. 59 (2) (2011) 582–589, http://dx.doi.org/10.1016/j.actamat.2010.09.062.

[25] E. Jiran, C.V. Thompson, Capillary instabilities in thin films, J. Electron. Mater. 19 (1990) 1153–1160, http://dx.doi.org/10.1007/BF02673327.

[26] W. Kan, H. Wong, Fingering instability of a retracting solid film edge, J. Appl. Phys. 97 (4) (2005) 043515, http://dx.doi.org/10.1063/1.1845579.

[27] C. Kennefick, R. Raj, Copper on sapphire: Stability of thin films at 0.7 tm, Acta Metall. 37 (11) (1989) 2947–2952, http://dx.doi.org/10.1016/0001-6160(89)90329-5.

[28] E. Shaffir, I. Riess, W. Kaplan, The mechanism of initial de-wetting and detachment of thin Au films on YSZ, Acta Mater. 57 (1) (2009) 248–256, http://dx.doi.org/10.1016/j.actamat.2008.09.004.

[29] H. Galinski, T. Ryll, L. Schlagenhauf, L.J. Gauckler, P. Stender, G. Schmitz, Hillock formation of pt thin films on single-crystal yttria-stabilized zirconia, Phys. Rev. B 85 (2012) 125408, http://dx.doi.org/10.1103/PhysRevB.85.125408.

[30] T. Frolov, W. Boettinger, Y. Mishin, Atomistic simulation of hillock growth, Acta Mater. 58 (16) (2010) 5471–5480, http://dx.doi.org/10.1016/j.actamat.2010.06.023.

[31] S.-J. Hwang, J.-H. Lee, C.-O. Jeong, Y.-C. Joo, Effect of film thickness and annealing temperature on hillock distributions in pure Al films, Scr. Mater. 56 (1) (2007) 17–20, http://dx.doi.org/10.1016/j.scriptamat.2006.09.001.

[32] A. Gladkikh, Y. Lereah, E. Glickman, M. Karpovski, A. Palevski, J. Schubert, Hillock formation during electromigration in Cu and Al thin films: Three-dimensional grain growth, Appl. Phys. Lett. 66 (10) (1995) 1214–1215, http://dx.doi.org/10.1063/1.113240.

[33] S. Sharma, J. Spitz, Hillock formation, hole growth and agglomeration in thin silver films, Thin Solid Films 65 (3) (1980) 339–350, http://dx.doi.org/10.1016/0040-6090(80)90244-8.

[34] H.-J. Nam, D.-K. Choi, W.-J. Lee, Formation of hillocks in pt/ti electrodes and their effects on short phenomena of PZT films deposited by reactive sputtering, Thin Solid Films 371 (1–2) (2000) 264–271, http://dx.doi.org/10.1016/S0040-6090(00)00970-6.

[35] W. Boettinger, C. Johnson, L. Bendersky, K.-W. Moon, M. Williams, G. Stafford, Whisker and hillock formation on Sn, Sn–Cu and Sn–Pb electrodeposits, Acta Mater. 53 (19) (2005) 5033–5050, http://dx.doi.org/10.1016/j.actamat.2005.07.016.

[36] C.V. Thompson, Solid-state dewetting of thin films, Annu. Rev. Mater. Res. 42 (1) (2012) 399–434, http://dx.doi.org/10.1146/annurev-matsci-070511-155048.

[37] C.M. Müller, R. Spolenak, Dewetting of Au and AuPt alloy films: A dewetting zone model, J. Appl. Phys. 113 (9) (2013) 094301, http://dx.doi.org/10.1063/1.4794028.

[38] F. Leroy, F. Cheynis, T. Passanante, P. Müller, Dynamics, anisotropy, and stability of silicon-on-insulator dewetting fronts, Phys. Rev. B 85 (2012) 195414, http://dx.doi.org/10.1103/PhysRevB.85.195414.

[39] E. Jiran, C. Thompson, Capillary instabilities in thin, continuous films, Thin Solid Films 208 (1) (1992) 23–28, http://dx.doi.org/10.1016/0040-6090(92)90941-4.

[40] P. Mueller, R. Kern, Equilibrium nano-shape change induced by epitaxial stress: effect of surface stress, Appl. Surf. Sci. 164 (1–4) (2000) 68–71, http://dx.doi.org/10.1016/S0169-4332(00)00327-5.

[41] F.-H. Lu, M.L. Newhouse, R. Dieckmann, J. Xue, Platinum—a non-inert material reacting with oxides, Solid State Ion. 75 (1995) 187–192, http://dx.doi.org/10.1016/0167-2738(94)00147-K.

[42] M. Köhl, K. Gindele, U. Frei, T. Häuselmann, Accelerated ageing test procedures for selective absorber coatings including lifetime estimation and comparison with outdoor test results, Sol. Energy Mater. 19 (35) (1989) 257–313, http://dx.doi.org/10.1016/0165-1633(89)90011-7.

[43] H. Mantz, K. Jacobs, K. Mecke, Utilizing Minkowski functionals for image analysis: A marching square algorithm, J. Stat. Mech. Theory Exp. 2008 (12) (2008) P12015.

[44] K. Jacobs, R. Seemann, K. Mecke, Statistical Physics and Spatial Statistics, Springer, Berlin, 2000, http://dx.doi.org/10.1007/3-540-45043-2_4.

[45] J. Becker, G. Grun, R. Seemann, H. Mantz, K. Jacobs, K.R. Mecke, R. Blossey, Complex dewetting scenarios captured by thin-film models, Nat. Mater. 2 (1) (2003) 59–63, http://dx.doi.org/10.1038/nmat788.

[46] K.R. Mecke, Morphology of spatial patterns – porous media, spinodal decomposition and dissipative structures, Acta Phys. Pol. B 28 (8) (1997) 1747–1782.

[47] Y. Oono, S. Puri, Computationally efficient modeling of ordering of quenched phases, Phys. Rev. Lett. 58 (1987) 836–839, http://dx.doi.org/10.1103/PhysRevLett.58.836.

[48] S. Puri, Y. Oono, Study of phase-separation dynamics by use of cell dynamical systems. II. Two-dimensional demonstrations, Phys. Rev. A 38 (1988) 1542–1565, http://dx.doi.org/10.1103/PhysRevA.38.1542.

[49] M. Bahiana, Y. Oono, Cell dynamical system approach to block copolymers, Phys. Rev. A 41 (1990) 6763–6771, http://dx.doi.org/10.1103/PhysRevA.41.6763.

[50] L.-T. Yan, X.-M. Xie, Computational modeling and simulation of nanoparticle self-assembly in polymeric systems: Structures, properties and external field effects, Prog. Polym. Sci. 38 (2) (2013) 369–405, http://dx.doi.org/10.1016/j.progpolymsci.2012.05.001.

[51] M. Pinna, A. Zvelindovsky, Large scale simulation of block copolymers with cell dynamics, Eur. Phys. J. B 85 (2012) 1–18, http://dx.doi.org/10.1140/epjb/e2012-20968-6.

[52] Y. Oono, S. Puri, Study of phase-separation dynamics by use of cell dynamical systems. I. Modeling, Phys. Rev. A 38 (1988) 434–453, http://dx.doi.org/10.1103/PhysRevA.38.434.

[53] S.R. Ren, I.W. Hamley, Cell dynamics simulations of microphase separation in block copolymers, Macromolecules 34 (1) (2001) 116–126, http://dx.doi.org/10.1021/ma000678z.

[54] J.W. Cahn, Phase separation by spinodal decomposition in isotropic systems, J. Chem. Phys. 42 (1) (1965) 93–99, http://dx.doi.org/10.1063/1.1695731.

[55] U. Thiele, M.G. Velarde, K. Neuffer, Dewetting: Film rupture by nucleation in the spinodal regime, Phys. Rev. Lett. 87 (1) (2001) 016104, http://dx.doi.org/10.1103/PhysRevLett.87.016104.

[56] U. Thiele, Open questions and promising new fields in dewetting, Eur. Phys. J. E 12 (2003) 409–416, http://dx.doi.org/10.1140/epje/e2004-00009-4.